Ogata and Tsuruoka *Earth, Planets and Space* (2016) 68:44
DOI 10.1186/s40623-016-0410-8

Earth, Planets and Space
a SpringerOpen Journal

LETTER

Open Access

Statistical monitoring of aftershock sequences: a case study of the 2015 Mw7.8 Gorkha, Nepal, earthquake

Yosihiko Ogata[1,2*] and Hiroshi Tsuruoka[2]

Abstract

Early forecasting of aftershocks has become realistic and practical because of real-time detection of hypocenters. This study illustrates a statistical procedure for monitoring aftershock sequences to detect anomalies to increase the probability gain of a significantly large aftershock or even an earthquake larger than the main shock. In particular, a significant lowering (relative quiescence) in aftershock activity below the level predicted by the Omori–Utsu formula or the epidemic-type aftershock sequence model is sometimes followed by a large earthquake in a neighboring region. As an example, we detected significant lowering relative to the modeled rate after approximately 1.7 days after the main shock in the aftershock sequence of the Mw7.8 Gorkha, Nepal, earthquake of April 25, 2015. The relative quiescence lasted until the May 12, 2015, M7.3 Kodari earthquake that occurred at the eastern end of the primary aftershock zone. Space–time plots including the transformed time can indicate the local places where aftershock activity lowers (the seismicity shadow). Thus, the relative quiescence can be hypothesized to be related to stress shadowing caused by probable slow slips. In addition, the aftershock productivity of the M7.3 Kodari earthquake is approximately twice as large as that of the M7.8 main shock.

Keywords: Epidemic-type aftershock sequence (ETAS) model, Omori–Utsu formula, Change-point, Probability gain, GUI software package XETAS, Relative quiescence, Seismicity shadow

Background

On April 25, 2015, a strong earthquake of Mw7.8 occurred along the Himalayan front close to Kathmandu, Nepal. Seventeen days after the main shock, the largest aftershock of May 12, the M7.3 Kodari earthquake, occurred in the eastern extension of the primary aftershock zone. The dip angle of the rupture fault zone is similar to that of the main fault zone on the plate boundary between the Indian and Eurasian plates.

The global probability forecast of the aftershocks of this earthquake (Michael et al. 2015) was implemented on the basis of near-real-time data of the National Earthquake Information Center (NEIC), refer to Page et al. (2015) for the method and procedure for the near-real-time global forecast. The initial forecast used the Reasenberg and Jones (1989) model with generic parameters of the region, which combine the Omori–Utsu law for the decay of aftershock frequency (Omori 1894; Utsu 1961) and the Gutenberg–Richter law for magnitude frequency (Gutenberg and Richter 1944). The model was subsequently updated to reflect a lower productivity and higher decay rate based on the observed aftershocks. This proved to be consistent with the main topic addressed in this paper. In fact, the forecast of the size distribution of aftershocks due to the Reasenberg–Jones predictor assumes the Gutenberg–Richter law. However, when precursory anomalies that can raise the probability gain of a large earthquake were detected, the probability forecast of the M7.3 aftershock was significantly small using this predictor only.

Retrospectively, we think that the forecast in this case could have yielded a higher likelihood of large-magnitude aftershocks than that predicted under the

*Correspondence: ogata@ism.ac.jp
[1] The Institute of Statistical Mathematics, 10-3 Midori-cho, Tachikawa, Tokyo 190-8562, Japan
Full list of author information is available at the end of the article

Gutenberg–Richter law. Relevant to this issue, Utsu (1979) and Aki (1981) emphasized the role of seismic anomalies in predicting the enhancement of the likelihood (probability gain) of having a substantially larger earthquake than the secular probability of the same size of earthquake. After the appearance of an anomaly, we need to evaluate the probability that it will be a precursor to a large earthquake; i.e., we need to forecast whether the probability in a space–time zone will increase to an extent, relative to that of the reference probability. Hence, it is desirable to search for anomalous phenomena that enhance the probability gains.

Seismic quiescence has attracted attention as a precursor candidate of large earthquakes (Inouye 1965; Utsu 1968; Ohtake et al. 1977; Wyss and Burford 1987; Kisslinger 1988). This anomaly concept is extended to include aftershock activity that can be significantly lower than the prediction of the Omori–Utsu formula (Matsu'ura 1986) or than the epidemic-type aftershock sequence model (ETAS model; Ogata 1988, 1992, 2001a, for example). The quiescence relative to the ETAS model is useful for the detailed description of aftershock sequences as well as general seismicity. Development of the statistical models and analysis methods of aftershock sequences can be found in Utsu et al. (1995).

From comprehensive study, the retrospective statistical results from Japanese data (Ogata 2001a) suggest that the probability gain of having another large earthquake of a similar size to the main shock becomes several times greater relative to the normal probability if the aftershock activity shows significant lowering. Therefore, it is necessary to pay careful attention to anomalous activity by monitoring the aftershock sequence, especially in the early stage.

Methods

Statistical models to monitor aftershock sequences

Short-term probability prediction of an earthquake of magnitude M_z or larger in a near-future period $(t, t + \mathrm{d}t)$ is given by $\lambda_\theta(t|H_t)\,\mathrm{d}t$ where $\lambda_\theta(t|H_t)$ is the history-dependent occurrence rate, for example, the ETAS model developed by Ogata (1985, 1988, 1989)

$$\lambda_\theta(t|H_t) = \mu + \sum_{\{i:0\le t_i<t\}} K_0 \mathrm{e}^{\alpha(M_i-M_z)} \Big/ (t - t_i + c)^p, \quad (1)$$

where $t = 0$ is the main shock time of the aftershock observation and M_z represents the reference magnitude (i.e., the main shock magnitude) of earthquakes to be treated in the dataset. M_i and t_i indicate the magnitude and the occurrence time of the ith earthquake, respectively, and H_t represents the occurrence series of earthquakes (t_i, M_i) before time t. The parameter set θ thus consists of five elements (μ, K_0, c, α, p). In fact, the second term of Eq. (1) is a weighted superposition of the Omori–Utsu empirical function (Utsu 1961) for aftershock decay rates;

$$\lambda(t) = K/(t + c)^p, \quad (2)$$

where t is the elapsed time from the occurrence of a main shock.

These parameters are obtained by maximizing the log-likelihood function (Ogata 1983, 1988, 1989) with respect to the parameter set θ. The log-likelihood function of the ETAS model,

$$\ln\, L(\theta; S, T) = \sum_{\{i:S<t_i<T\}} \ln\, \lambda_\theta\left(t_i|H_{t_i}\right) - \int_S^T \lambda_\theta(t|H_t)\mathrm{d}t, \quad (3)$$

is maximized with respect to the parameter set $\theta = (\mu, K, c, \alpha, p)$. Here, 'ln' is a natural logarithm, and $\{(t_i, M_i), M_i \ge M_c; i = 1, 2, \ldots\}$ are occurrence times and magnitudes of earthquakes in the target time interval $[S, T]$ for the fitting. Note here that the fitted data in the target interval $[S, T]$ do not contain the main shock and immediately following aftershocks during the period $[0, S)$, but that $\lambda_\theta(t|H_t)$ include the data of the main shock and aftershocks during the period $[0, S)$ as the preceding history. Note also that the Omori–Utsu model is not history dependent except for the elapsed time since the main shock, and it is possible to apply the same log-likelihood function as (3) with $\theta = (K, c, p)$. The obtained parameter values are called the maximum likelihood estimates (MLE).

The Reasenberg and Jones method combines the Omori–Utsu aftershock decay, Utsu productivity scaling (Utsu 1970), and Gutenberg–Richter magnitude distribution (Gutenberg and Richter 1944), such that $\lambda(t) \cdot 10^{-b(M-M_c)}$. Similarly, $\lambda(t|H_t) \cdot 10^{-b(M-M_c)}$ can yield a better forecast for the case of multiple sources of earthquake clustering.

In terms of prediction, the goodness of fit of the model is measured using the Akaike information criterion (AIC; Akaike 1973), which is described as

$$\mathrm{AIC}_{[S,T]} = -2\max \ln\, L(\theta; S, T) + 2k, \quad (4)$$

where $\ln L(\theta)$ represents the log likelihood (3) of the statistical model and k is the number of parameters to be estimated. With this criterion, the model with a smaller value of the AIC is expected to perform better prediction. The difference in the AIC values, ΔAIC, between the two competing models is useful, because $\exp\{-\Delta\mathrm{AIC}/2\}$ can be interpreted as the relative probability of how the model with the smaller AIC value is superior to the other, see the selected papers of Akaike (Parzen

et al. 1998). Hence, for an aftershock sequence, a simpler model with a smaller number of adjusted parameters will yield a smaller AIC value if the difference in the maximum log-likelihood values is smaller than 1.0. Therefore, we may sometimes assume fixed parameter values $\mu = 0$ or generic parameters such as $p = 1.0$ in the aftershock sequence to compare the AIC value of the ETAS model or the Omori–Utsu model.

When a seismicity change is suspected, we may look at the most likely candidate for the change-point time T_0 in a given period $[S, T]$. First, we separately fit suitable statistical models for the divided periods $[S, T_0]$ and $[T_0, T]$ (two-stage model), and then we compare their total performance against the model fitted over the whole period $[S, T]$ by the AIC. Then the most likely estimate of change-point should minimize

$$\mathrm{AIC}(T_0) = \mathrm{AIC}_{[S,T_0]} + \mathrm{AIC}_{[T_0,T]}, \tag{5}$$

or maximize the likelihood (e.g., Bansal and Ogata 2013)

$$\exp\{-\mathrm{AIC}(T_0)/2\} \propto L(\theta_1; S, T_0) \cdot L(\theta_2; T_0, T), \tag{6}$$

with respect to the change-point candidate parameter T_0, which can be called the MLE of the change-point with respect to the time.

Theoretical cumulative function and time transformation

Suppose that the parameter values $\theta = (\mu, K, c, \alpha, p)$ of the ETAS model (1) are given. Then the integral of the conditional intensity function,

$$\Lambda_\theta(t|H_t) = \int_S^t \lambda_\theta(u|H_u)\mathrm{d}u, \tag{7}$$

provides the expected cumulative number of earthquakes in the time interval $[S, t]$. The time transformation from t to τ is considered based on this cumulative intensity;

$$\tau = \Lambda(t|H_t) \tag{8}$$

transforms the ordinary occurrence times of aftershocks; $(t_1, t_2, \ldots, t_N)$ into the sequence $(\tau_1, \tau_2, \ldots, \tau_N)$ in the time interval $[0, \Lambda(T)]$, which we call the residual point process (RPP). If the model is a good approximation to the real seismicity, we expect its integrated function (7) and the empirical cumulative counts $N(t)$ of the observed earthquakes to be similar to each other. This implies that the transformed sequence (the RPP) appears to be a stationary Poisson process (uniformly distributed occurrence times) with unit intensity (occurrence rate) if the model is sufficiently correct, but it appears to be heterogeneous otherwise.

Let $N(\sigma, \tau)$ be the number of events in the interval (σ, τ) in the transformed time axis. If no change in aftershock activity occurs, the extrapolated RPP is also the standard stationary Poisson process with the same unit intensity, and the deviation $N(\tau_0, \tau) - (\tau - \tau_0)$ of the empirical cumulative function is approximately distributed according to the normal distribution $\mathbf{N}(0, \Delta\tau)$ where $\Delta\tau = \tau - \tau_0$. However, when the number of events $N(\sigma, \tau_0)$ in the target interval (σ, τ_0) is not large enough, the significance actually depends on the sample size, due to the estimation accuracy of the parameters for the transformation. Thus, taking such accuracy into consideration, the error distribution of $\Delta N(\tau_0, \tau)$ is modified to be $\mathbf{N}\big(0, \ \Delta\tau + (\Delta\tau)^2/N(\sigma, \tau_0)\big)$, derivation of which is provided in Appendix B of Ogata (1992). Hereafter we define the anomaly in the case where the empirical cumulative function deviates outside the parabola of 95 % significance $2\big\{\Delta\tau + (\Delta\tau)^2/N(\sigma, \tau_0)\big\}$.

The FORTRAN program package associated with manuals regarding the ETAS analysis is available to calculate the MLE of θ and also to visualize model performances (Ogata 2006c), which has been extended to the program package XETAS (Tsuruoka and Ogata 2015a, b) using graphical user interface (GUI).

Data and results

We first used the NEIC Preliminary Determination of Epicenters (PDE) for datasets of the on-fault aftershocks in the rectangular area bounded by the 84.4°E and 86.4°E meridians and 27.2°N and 28.4°N parallels obtained on May 13, 2015 (the day after the M7.3 Kodari earthquake; hereafter termed the first PDE data). Results similar to those of this study using this dataset were reported in early June 2015 at a workshop (Ogata 2015; Tsuruoka and Ogata 2015a). In addition, we used the second PDE data obtained on July 22, 2015 (Tsuruoka and Ogata 2015b), and herein we also incorporate the final datasets from the Advance National Seismic Network (ANSS) obtained on October 31, 2015.

We used the TSEIS visualization program package (Tsuruoka 1996) for selection of datasets from the catalogs. The identified aftershocks in the PDE catalog increase as time evolves, and the ANSS catalog includes about twice as many primary aftershocks before the M7.3 event as the first PDE data. In addition to the relocated epicenters and re-evaluated magnitudes of the same aftershocks, newly detected aftershocks are listed as time proceeds. Figure 1a, b shows such differences between the first PDE data and the ANSS data; as far as the sequences of occurrence times and magnitudes are concerned, the second PDE data and the ANSS data are almost identical.

We use the GUI program package XETAS (Tsuruoka and Ogata 2015a, b), efficiently implementing the above-mentioned methods in the following statistical analysis. The estimation results are summarized in Table 1.

First, as near-real-time monitoring, we analyze the primary aftershocks of the first PDE data until the

occurrence time of the largest aftershock of M7.3. The threshold magnitude is taken as M4.5 for completeness in the period from 1 h after the main shock occurrence time, as shown in Fig. 1. We apply the ETAS model and the Omori–Utsu model to this entire period. Table 1a indicates that the ETAS model fits better than the Omori–Utsu model according to the AIC values. The estimated decaying parameter p values of both the Omori–Utsu and ETAS models are seemingly quite large; this may be explained as follows.

By applying the ETAS model to the dataset for a whole target period, we preliminarily search a time interval in which change-points seem to exist, inspecting the deviations of the cumulative curve of the transformed time (8) from the straight line. We then calculate $\exp(-\Delta AIC/2)$ of the likelihood of change-point time (see "Methods"

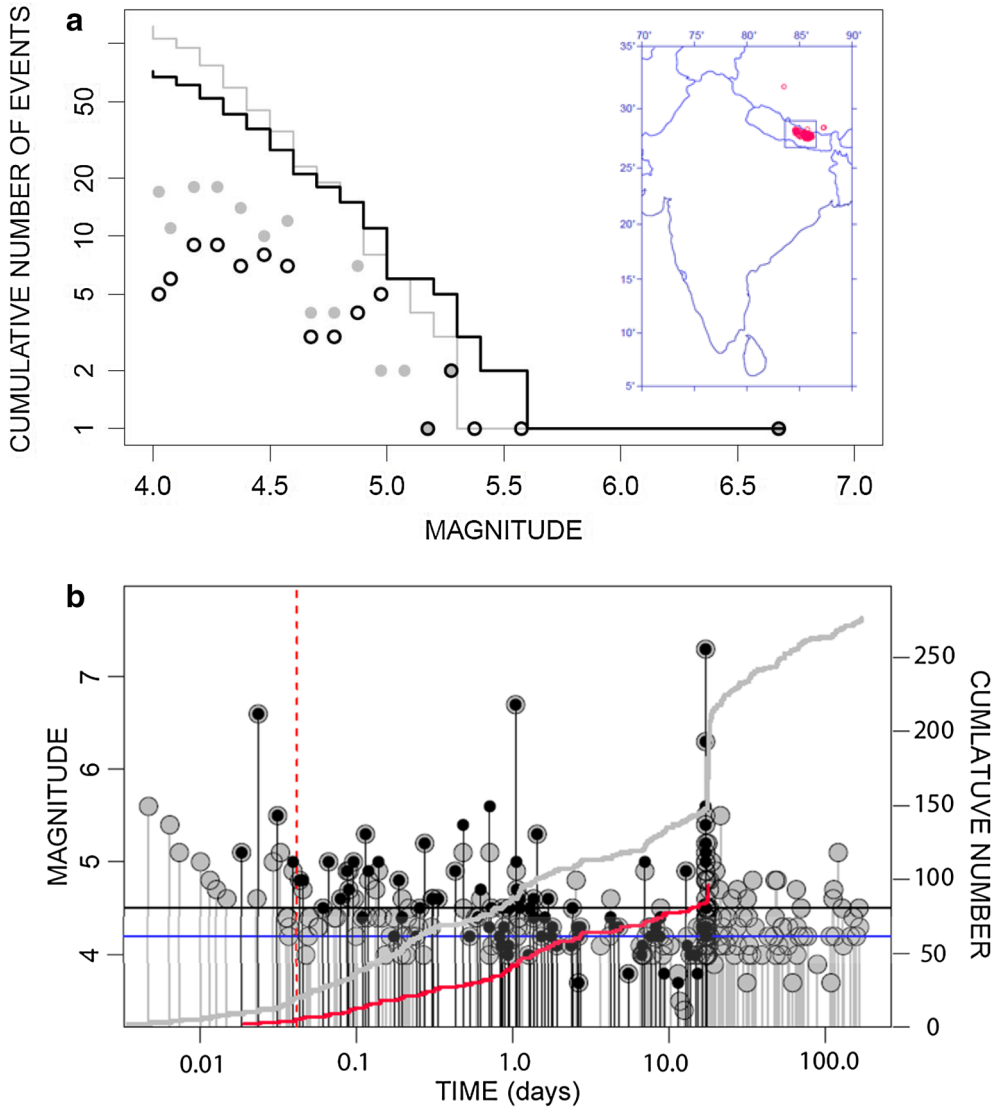

Fig. 1 Detected aftershocks and their magnitudes. **a** *Open circles* and *gray dots* indicate the frequencies of identified aftershocks against magnitudes for the period between the main shock and the M7.3 largest aftershock, listed in the PDE catalog at May 13, 2015, and the ANSS catalog at October 31, 2015, respectively. The *black* and *gray step* functions are the cumulative numbers of identified aftershocks from the largest magnitude to the lowest, corresponding to the magnitude frequencies. **b** Magnitude versus elapsed time from the main shock on a logarithmic scale. *Black* and *gray dots* correspond to the identified aftershocks in the PDE catalog at May 13, 2015, and the ANSS catalog, respectively. The cumulative numbers of detected aftershocks plotted in *red* and in *gray* correspond to those from the PDE and ANSS catalogs, respectively. The *black* and *blue horizontal lines* represent the levels of M4.5 and M4.2, respectively. The *red vertical dotted line* indicates the start time of the target interval for fitting the aftershock models

section above). Thus, as given in Table 1, the 1.7 days from the main shock occurrence are the most likely (MLE) candidate of change-point time. Incidentally, we cannot detect a significant local peak around the time (1.04 days) of the second largest aftershock of M6.7.

After the MLE of the change-point, the number of aftershocks of M4.5 and larger become markedly low, so we suspect that there was a change in the seismicity pattern at the time. According to Table 1a, the Omori–Utsu model with very high p value fits better than the ETAS model in the period from 1 h until the suspected change-point time (1.7 days) before the M7.3 aftershock. The difference in the AIC/2 values is small, and thus the simpler model is preferred for the prediction, probably due to the small number of events at this threshold magnitude. Figure 2a–c shows the best-fit models for the entire period (ETAS) and for the separate periods (the Omori–Utsu model and stationary Poisson model). Figure 2b, d shows the fit of the Omori–Utsu cumulative curve to the empirical cumulative function before the change-point at 1.7 days after the main shock and also show the deviation from the empirical cumulative function after the change-point. These show that about 20 potentially expected aftershocks of M4.5 or larger did not occur during the quiet period.

Next, to examine the stability of the above results, we also use the ANSS data for similar analysis of the aftershocks before the M7.3 event for various target periods and lower threshold magnitudes as described in Table 1b to ensure completeness of the datasets in accordance with Fig. 1. In these data from the ANSS catalog, the likely change-point estimate is also 1.7 days. The results of the O–U and the ETAS models are similar to each other according to Table 1b. For the primary aftershocks throughout the entire period until the M7.3 event, the

Table 1 MLE of the models and values of the AIC/2 for respective datasets

	Data	Models	Mc	Tstart	Tend	AIC/2	μ	K	c	α	p
(a)	PDE	ETAS	4.5	0.0417	17.0	−64.06	0.00	4.12	0.0571	2.08	1.59
	PDE	O–U	4.5	0.0417	17.0	−61.56	0.00	12.18	0.2870	–	1.95
	PDE	ETAS	4.5	0.0417	1.7	−73.77	0.00	7.50	0.0091	2.24	1.00
	PDE	O–U	4.5	0.0417	1.7	−74.47	0.00	11.16	0.0000	–	0.81
	PDE	Poisson	4.5	1.7	17.0	8.89	0.20	–	–	–	–
(b)	ANSS	ETAS	4.5	0.01	17.00	−142.58	0.00	5.95	0.0369	2.62	1.44
	ANSS	O–U	4.5	0.01	17.00	−141.38	0.00	7.74	0.0488	–	1.44
	ANSS	ETAS	4.5	0.01	1.70	−154.92	0.00	9.59	0.0055	2.85	1.00
	ANSS	O–U	4.5	0.01	1.70	−154.77	0.00	10.80	0.0067	–	1.00
	ANSS	ETAS	4.5	1.7	17.00	12.16	0.00	2.61	0.0000	Large	1.00
	ANSS	O–U	4.5	1.7	17.00	11.06	0.00	2.61	0.0000	–	1.00
	ANSS	ETAS	4.4	0.0417	17.00	−145.22	0.00	7.15	0.0595	2.38	1.63
	ANSS	O–U	4.4	0.0417	17.00	−142.29	0.00	11.77	0.1130	–	1.68
	ANSS	ETAS	4.4	0.0417	1.70	−156.86	0.00	12.62	0.0060	2.63	1.00
	ANSS	O–U	4.4	0.0417	1.70	−156.11	0.00	14.33	0.0004	–	1.00
	ANSS	ETAS	4.4	1.7	17.00	11.06	0.00	2.61	0.0000	Large	1.00
	ANSS	O–U	4.4	1.7	17.00	11.16	0.00	2.61	0.0000	–	1.00
(c)	ANSS	ETAS	4.2	0.0417	17.00	−221.34	0.00	11.14	0.0207	2.18	1.26
	ANSS	ETAS	4.2	0.0417	1.50	−228.12	0.00	10.47	0.0420	2.16	1.42
	ANSS	O–U	4.2	1.5	17.00	7.66	0.00	10.71	0.0000	–	1.00
	ANSS	ETAS	4.2	0.0417	1.70	−232.94	0.00	11.62	0.0344	2.20	1.33
	ANSS	O–U	4.2	1.7	17.00	11.96	0.00	9.99	–	–	1.00
	ANSS	ETAS	4.2	0.0417	2.00	−234.82	0.00	11.21	0.0381	2.18	1.36
	ANSS	O–U	4.2	2.0	17.00	13.78	0.00	9.81	–	–	1.00
	ANSS	ETAS	4.2	0.0417	3.00	−236.01	0.00	10.91	0.0419	2.19	1.40
	ANSS	O–U	4.2	3.0	17.00	15.16	0.00	9.80	–	–	1.00
(d)	ANSS	ETAS	4.2	0.0417	164.72	−294.23	0.00	12.64	0.0123	2.08	1.19
	ANSS	ETAS	4.2	0.0417	17.04	−221.34	0.00	11.14	0.0207	2.18	1.26
	ANSS	ETAS	4.2	17.04	164.72	−75.56	0.00	69.32	0.0541	4.43	1.41

'Tstart' and 'Tend' indicate the range of target intervals of respective datasets. 'O–U' is an abbreviation for the Omori–Utsu model. Blocks (a)–(d) provide the fitted results of the models for the same datasets but different setups, as cited in the text

ETAS model fits better than the Omori–Utsu model, and the p values of the both models are rather high, namely 1.4–1.7. In the target period before the suspected change-point, the ETAS model shows a slightly better fit than the Omori–Utsu model, possibly because of the increased data size, but the p values of the both models remain generic, namely $p = 1.0$ in this case. Figure 3 shows the case where the target interval is from 0.01 days (approximately 15 min) until the suspected change-point at 1.7 days and with a threshold magnitude of M4.5. Relative quiescence is also likely to have occurred. Figure 3b, d also shows that about 20 potentially expected aftershocks of M4.5 or larger did not occur during the quiet period.

We further examined aftershocks from the ANSS catalog with the possible lowest homogeneous threshold magnitude of $M = 4.2$ in the period from 1 h until the M7.3 event, in accordance with Fig. 1. The most likely change-point candidate in this case is 2.0 elapsed days as given in Table 1c, but Fig. 4a, b shows that the aftershock activity after day 2 until the M7.3 event appears to have decayed normally as predicted. Hence, we may conclude that aftershock activity with $M \geq 4.2$ was normal throughout the entire period before the M7.3 event.

We examine whether any seismicity change occurred after the M7.3 event. The results of the ETAS fitting are given in Table 1d, and Fig. 4c, d shows that secondary aftershocks of $M \geq 4.2$ occurred significantly more often than predicted. From the plot of magnitude versus transformed time in Fig. 4d, there are a substantial number of missing aftershocks of $M \geq 4.2$ immediately after the M7.3 event. Hence, the actual number of secondary aftershocks was about twice as large as that predicted from the primary aftershock activity, and the aftershock productivity of the M7.3 event was twice as large as that of the main shock of M7.8. This finding implies that a single ETAS model does not always provide a proper forecast of the secondary aftershock sequence from the fit of the primary aftershock sequence, as illustrated in Fig. 4. This is because the ETAS model assumes the same productivity coefficient for every earthquake, but this is not always true in real seismicity (cf. Ogata 2001b).

It is also worthwhile to assess the space–time evolution of aftershock occurrences in Fig. 5 with respect to the transformed time using the Omori–Utsu cumulative curves. Although the detection rate of smaller aftershocks gradually increased with elapsed time, we used all the located aftershocks in both the near-real-time PDE catalog and the ANSS catalog and fitted the Omori–Utsu model to them to obtain detrended space–time aftershock occurrences with respect to transformed time. Here, we should note that such space–time occurrence is not always uniform with respect to the transformed time at any place, and nonuniform occurrence times of aftershock activity are often observed in some local regions with respect to the transformed time, such as transient lowering or activation (Ogata 2010a).

On the basis of the space–time plots of aftershocks from both catalogs including the transformed time until the M7.3 event in Fig. 5, we can conclude that the spatial distribution of the primary aftershocks was heterogeneous, as detailed below.

The plots of epicenter longitudes against transformed times indicate that the eastern part of the aftershock zone was more active than the western part, which includes the main shock; and the western sparser area of aftershocks expanded toward the east. In the shrinking active eastern zone, the M6.7 large aftershock occurred on April 26 (approximately 1 day after the main shock), and then the active zone became quiet until the appearance of densely populated smaller aftershocks near the location of the M7.3 event around 86.1°E. Relevantly, Matsu'ura (1986) commented that relative quiescence is probably activated just before large aftershocks; hence, these may represent some type of foreshocks of a large aftershock.

The plot of epicenter latitudes against transformed times in Fig. 5 indicates that the early aftershocks near the main shock were very sparse but recovered to some extent in about a day. This result suggests that triggering of aftershocks around the main shock was delayed. Then the northern region become quiet and also shows expansion toward the eastern end near the Kodari earthquake of M7.3.

Discussion

Seismicity quiescence and empirical medium-term forecasting

Although quite a number of years have passed since seismologists said that seismic quiescence could be effective in prediction, there have not been many examples of quiescence that have been pointed out in advance of a major earthquake. Also, the number and conditions of the parameters that describe the involved relationship between the space–time domain of quiescence and potential large earthquakes for general seismic activity are too large to yield a definite answer.

Notwithstanding, it may be easier to address the issue by restricting the subject to aftershock sequences. From the near-real-time aftershock data, it is sometimes possible to observe probable relative quiescence that may follow a large aftershock with a higher probability gain than the case of normally decaying aftershock activity. It will be desirable to know the probability gain of a specified size of large aftershock. When aftershocks occur significantly less frequently in comparison with the number predicted by the Omori–Utsu or the ETAS model when

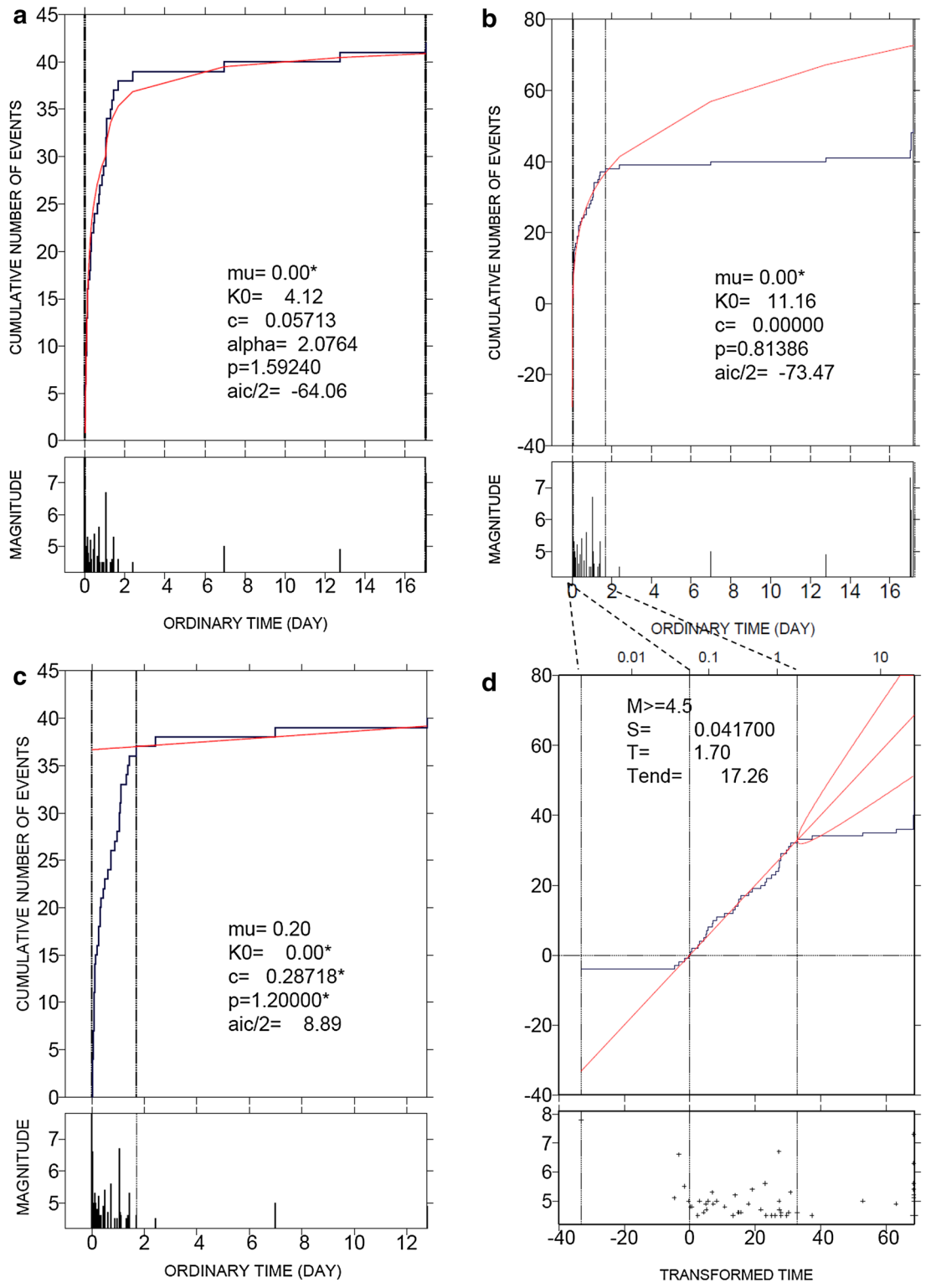

Fig. 2 Fit comparisons for seismicity based on the PDE catalog. Aftershock data of $M \geq 4.5$ were obtained from the PDE catalog for the date May 13, 2015. Their empirical cumulative function and magnitudes are plotted versus the ordinary occurrence times (**a**, **b**, **c**) and the transformed time (**d**) in the *horizontal axis*. **a** Theoretical cumulative (*red*) curves of the fitted ETAS model for the target entire time interval from 0.0417 day (1 h) after the main shock until the M7.3 largest aftershock. **b** As in (**a**) except that the target interval is the earlier time interval, divided at the elapsed time of 1.7 days (*vertical thin line*) after the main shock. **c** As in (**b**) except that the target is the later time interval, after 1.7 days. **d** As (**b**) except for including transformed time in addition to the parabola for the 95 % confidence ranges of the extrapolated curve

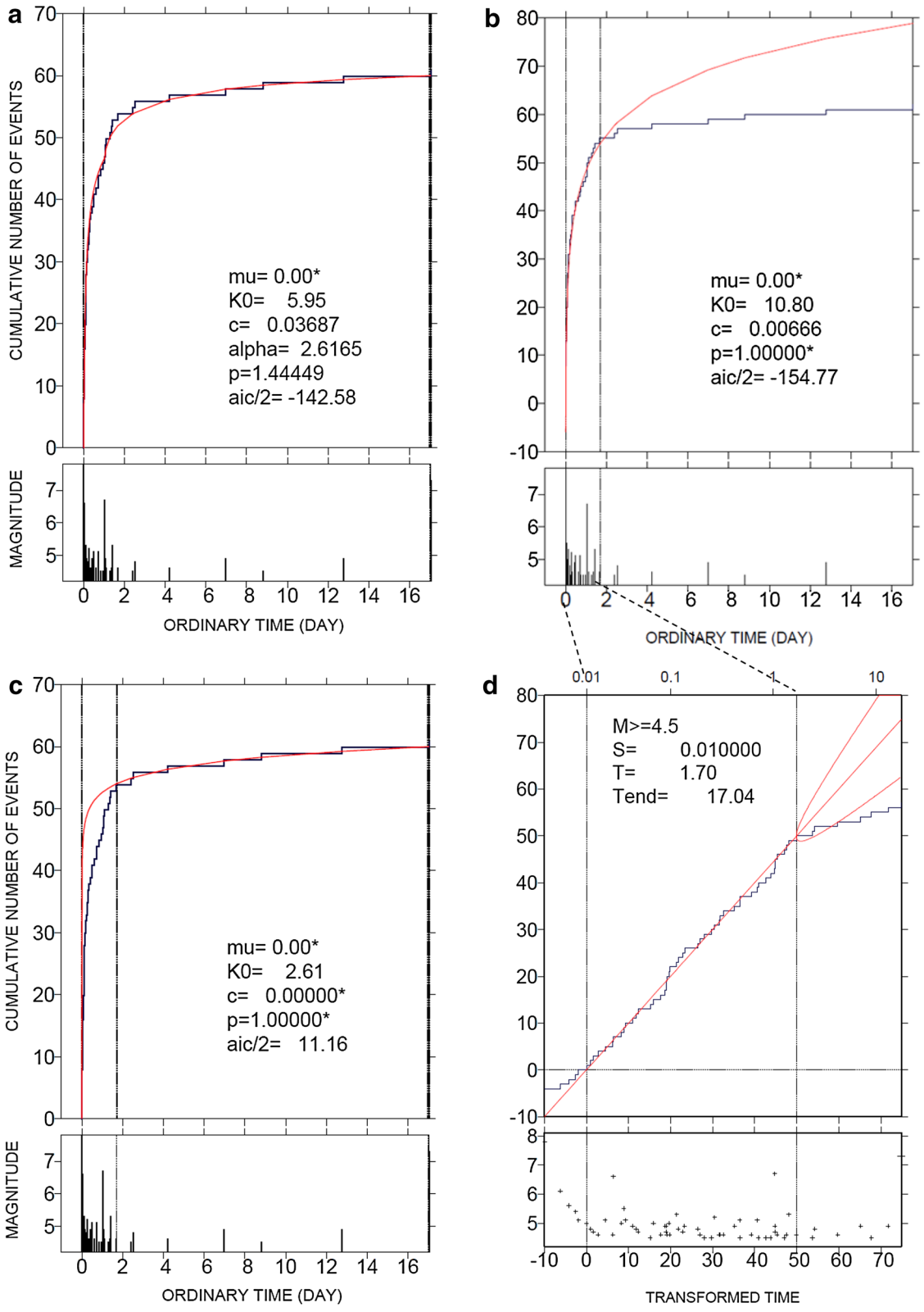

Fig. 3 Fitting comparisons of seismicity based on the ANSS catalog. **a**–**d** The same plots as the corresponding panels of Fig. 2, except that the starting time is 0.01 day (approximately 15 min)

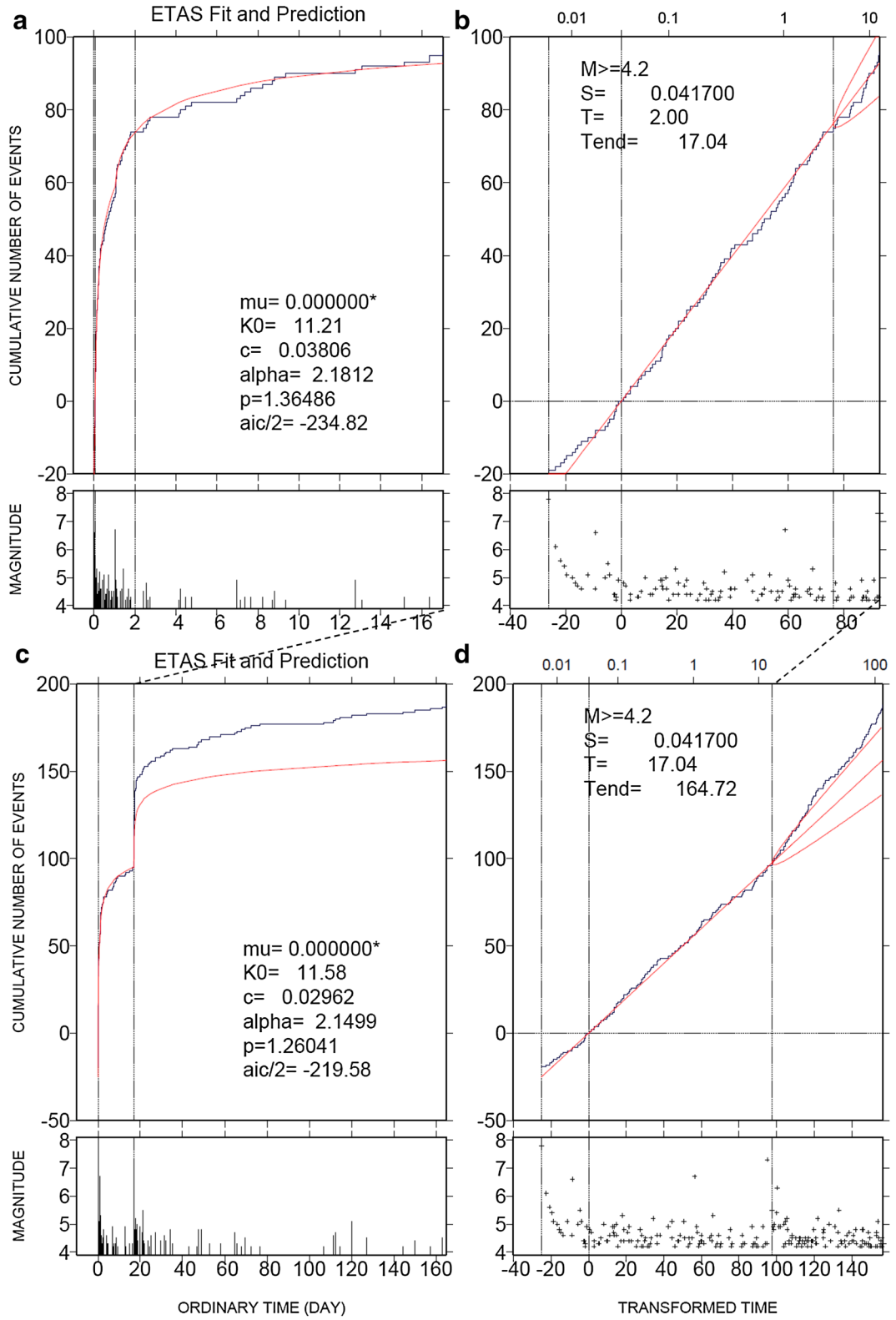

Fig. 4 Overall activity of aftershocks of $M \geq 4.2$. Empirical (*black*) and theoretical (*red*) cumulative functions and magnitudes plotted against ordinary time (**a**, **c**) and transformed times (**b**, **d**). **a**, **b** The ETAS fitting in the target interval from 1 h until 2 days and then extrapolated until the M7.3 event; **c**, **d** The ETAS fitting in the target interval from 1 h until the M7.3 event and then extrapolated until the end of October 2015. The parabolas in **b**, **d** represent the 95 % confidence ranges of the extrapolated curve

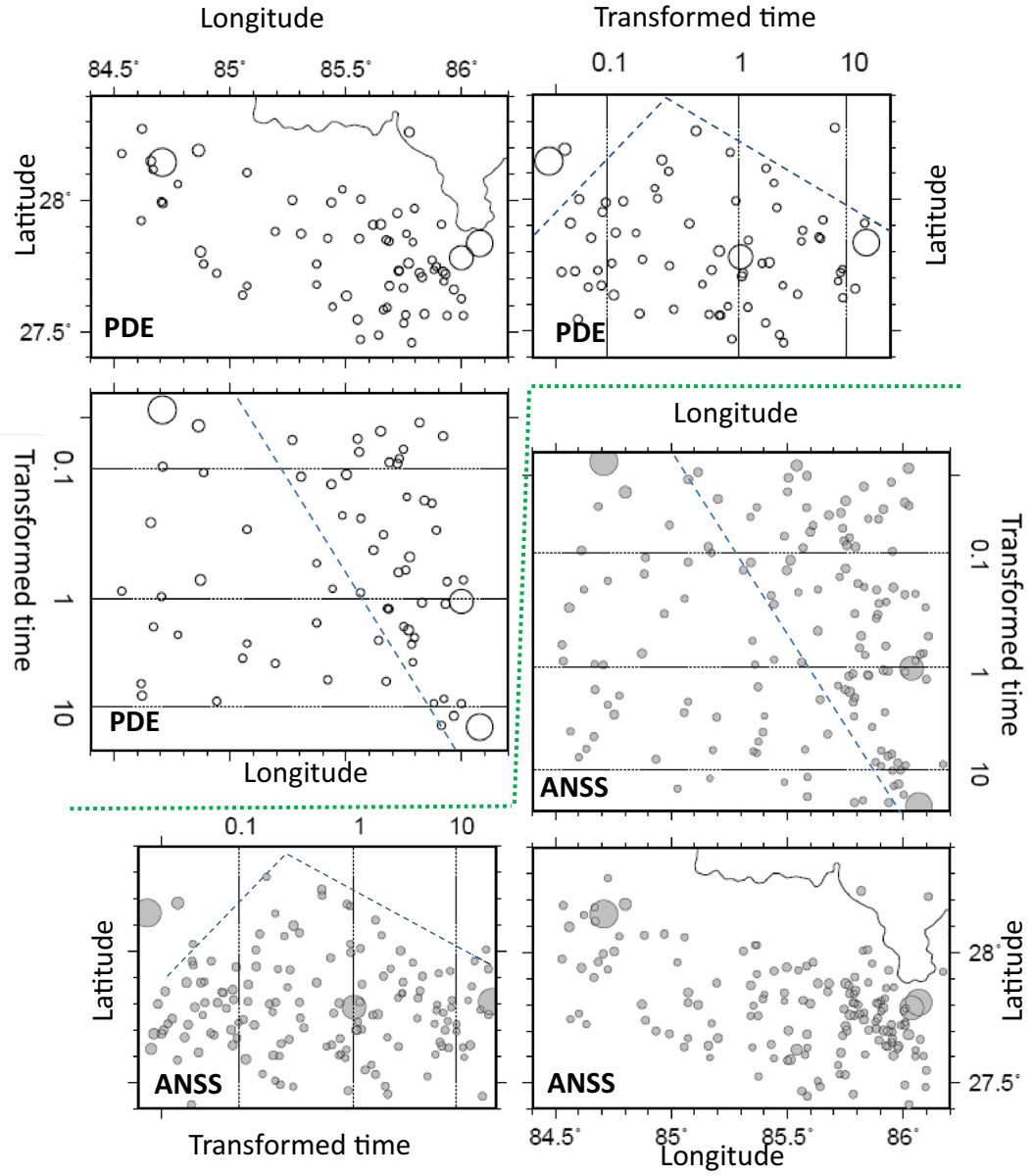

Fig. 5 Detrended space–time plot of the primary aftershocks. Epicenter locations and space–time plots of the detected aftershocks in the near-real-time PDE catalog (*upper triangle array panels*) and the ANSS catalog (*lower triangle array panels*) against transformed time for the period between the main shock and the M7.3 event. The respective transformed times are obtained using the Omori–Utsu function that is fitted their detected aftershock data throughout the entire period from the main shock until the M7.3 event. Epicenters of the located aftershocks (*top left panel* and *bottom right panel*), epicenter latitude against transformed time (*top right panel* and *bottom left panel*), and transformed time against epicenter longitude (*middle row panels*). The sizes of the *circles* indicate the magnitude. The large circles mark the epicenters of the M7.8 main shock, the M7.3 largest aftershock, and the M6.7 aftershock of April 26, 2015

aftershocks are attenuated as expected by the model, we empirically expect a higher possibility of a significantly large aftershock, which will probably occur on a fault boundary.

This type of empirical probability gain has been obtained in a large number of case studies. For example, Ogata (2001a) investigated 76 aftershock sequences in Japan, detected relative quiescence in 34 cases, and evaluated the probability gain of a large earthquake as follows. First, if a large earthquake has occurred in a particular location, the probability per unit area that another earthquake of similar magnitude will occur in the vicinity is greater than the probability for a distant area. This is the result of empirical

statistics regarding the self-similarity feature (inverse-power law correlations) and also physically suggests that the neighboring earthquake will be more likely to be induced by a sudden stress change on the periphery because of the abrupt slip of the earthquake. Moreover, if aftershock activity becomes relatively quiet, it becomes more likely that large aftershocks will occur around the boundary of the aftershock area. Furthermore, if relative quiescence lasts for a sufficiently long time (more than a few months), the probability of another earthquake of similar magnitude will increase to about three times the probability gain within 6 years in the vicinity of the aftershock area (within 200 km distance). Similar evaluations may be carried out to obtain the probability gain for an aftershock that is larger than magnitude $M_0 - 0.5$ for a main shock of magnitude M_0, for example, in a shorter period of relative quiescence.

If the detection rates of aftershocks regarding magnitudes are same throughout the target period, we can make use of a homogeneous dataset under a smaller threshold magnitude instead of the dataset of completely detected threshold magnitudes to allow less-uncertain inference and prediction (Ogata and Katsura 1993, 2006). It is also desirable to recover information on missing aftershocks using modeling of detection rates, particularly in the early stage of aftershocks (Omi et al. 2013, 2014a, b).

The physical meaning of seismic quiescence

When a significant quiescence has been detected, it is necessary to question whether and how this leads to large earthquakes, if any occur. There are various conditions such as tectonics and stress fields that can be used for quantitative representation of the quiescence phenomenon to be addressed. A comprehensive physical study of the seismic quiescence preceding a large earthquake is essential for enhancement of the probability gain of the anomaly. These elements must be incorporated to achieve a predicted probability that exceeds the predictions of typical statistical models. Specifically, using the model, some retrospective case studies (Ogata 2013; and references therein) have been concerned with the phenomenon that the stress shadow (e.g., Harris 1998) inhibits normal aftershock activity.

As discussed in Ogata (2005a, b, c, 2006a, b, 2007, 2010b, 2011), Ogata et al. (2003), Kumazawa et al. (2010), and Kumazawa and Ogata (2013), we should consider and demonstrate the relationship of seismicity lowering (seismicity shadow) in the space–time aftershock occurrence patterns together with slow slips on the plate boundary using geodetic studies for the present Gorkha case (e.g., Avouac et al. 2015; Zhang et al. 2015; Fielding et al. 2015; Grandin 2015; Ingleby et al. 2015). Specifically, scenarios explaining the relative quiescence can rely on the seismicity rate change based on the rate-and-state friction law of Dieterich (1994) as the quantitative basis of the triggering (Ogata et al. 2003; Ogata 2004, 2010a; Ogata and Toda 2010).

Although transient slow slip is promising as a possible precursor to a strong earthquake in medium-term and short-term predictions, this should in some way be discriminated from habitual slip or postseismic slip. It is necessary to identify these types of slip statistically based on space–time seismicity patterns to allow empirical evaluation of the probability gain of large earthquakes. Furthermore, if it is possible to identify the precursory slips more clearly by constraining the physical setup based on other data, such as various kinds of geodetic observations, the probability gain may become higher.

Conclusions

Operational quasi-real-time statistical monitoring of anomalies of aftershock sequences should be implemented together with probability forecasting based on real-time earthquake datasets using either the Omori–Utsu model or the ETAS model. Diagnostic analysis based on fitting the models is helpful in detecting various anomalies, such as the seismic quiescence, relative to the models; such an anomaly can enhance the probability gain of the occurrence of neighboring strong earthquakes. In this study, we illustrate this type of statistical monitoring for the early aftershock sequence of the Gorkha earthquake of M7.8 using the PDE datasets and the ANSS catalog.

We recommend that readers use the XETAS program (Tsuruoka and Ogata 2015a, b), which requires a small amount of memory and is a robust software kit with a GUI interface for making quick estimates of the ETAS and Omori–Utsu models and for various diagnostic analyses. This package also includes display of space–time plots of aftershocks relative to the transformed time; this allows exploration of the transient part of a relatively quiet area (seismicity shadow) and activated area, which is useful to identify the stress-shadow area and the area of stress increase, respectively, and eventually to search for suspected aseismic slips on a fault or its vicinity.

Moreover, it is necessary to estimate the uncertainty in the nature and urgency of abnormal phenomena relative to their roles as precursors to major earthquakes. For this purpose, it is necessary to study a large number of normal and anomalous cases for potential precursory links to large earthquakes. Thus, incorporation of this information in the design of a prediction model for probability that exceeds the underlying probability is important. Also, such comprehensive monitoring experiments

with examination of speculative physical scenarios may eventually clarify the tectonic mechanisms that cause significantly large aftershocks with higher probability gains than that of ordinary aftershock activity, which follows the empirical laws of aftershocks. In conclusion, based on such quantitative studies, we hope that it will eventually be possible to say that the probability of the occurrence of a large earthquake in a certain period and a certain region has increased by a certain extent compared with the reference probability.

Abbreviations

AIC: Akaike information criterion; ANSS: Advance National Seismic Network; ETAS model: epidemic-type aftershock sequence model; GUI: Graphical user interface; MLE: maximum likelihood estimates; NEIC: National Earthquake Information Center; O–U model: Omori–Utsu model; PDE: Preliminary Determination of Epicenters; RPP: residual point process; XETAS: X-windows-based ETAS applications.

Authors' contributions

YO organized the study, carried out the analysis, and drafted the manuscript. HT has written the XETAS programs, modified and extended the functions for the current research, and checked the results and manuscript. Both authors read and approved the final manuscript.

Author details

[1] The Institute of Statistical Mathematics, 10-3 Midori-cho, Tachikawa, Tokyo 190-8562, Japan. [2] Earthquake Research Institute, The University of Tokyo, 1-1-1 Yayoi, Bunkyo-ku, Tokyo 113-0032, Japan.

Acknowledgements

We have benefited from the editor and anonymous reviewers for their constructive comments which clarified the present paper. The present study was supported by JSPS KAKENHI Grant 26240004.

Competing interests

The authors declare that they have no competing interests.

Received: 2 December 2015 Accepted: 11 February 2016
Published online: 17 March 2016

References

Akaike H (1973) Information theory and an extension of the maximum likelihood principle. In: Petrov BN, Csaki F (eds) Proceedings of 2nd international symposium on information theory. Akademiai Kiado, Budapest, pp 267–281. Republished edition: Kotz S, Johnson NL (eds) (1992) Breakthroughs in Statistics, vol 1, foundations and basic theory. Springer, New York, pp 610–624

Aki K (1981) A probabilistic synthesis of precursory phenomena. In: Simpson DW, Richards PG (eds) Earthquake prediction. Maurice Ewing series, 4. American Geophysical Union, Washington, pp 566–574

Avouac JP, Meng L, Wei S, Wang T, Ampuero JP (2015) Lower edge of locked Main Himalayan Thrust unzipped by the 2015 Gorkha earthquake. Nat Geosci 8:708–711

Bansal AR, Ogata Y (2013) A non-stationary epidemic type aftershock sequence model for seismicity prior to the December 26, 2004 M9.1 Sumatra–Andaman Islands mega-earthquake. J Geophys Res 118:616–629. doi:10.1002/jgrb.50068

Dieterich J (1994) A constitutive law for rate of earthquake production and its application to earthquake clustering. J Geophys Res 99:2601–2618

Fielding EJ, Liang C, Agram PS, Sangha SS, Huang MH, Samsonov SV, Owen SE, Moore AW, Rodriguez-Gonzalez F, Minchew BM (2015) Geodetic imaging of the coseismic and postseismic deformation from the 2015 Mw 7.8 Gorkha Earthquake and Mw 7.3 aftershock in Nepal with SAR and GPS. 2015 Fall Meeting of American Geophysical Union, S43D-2824

Grandin R (2015) Postseismic deformation following the April 2015 M7.8 Nepal earthquake measured using sentinel-1A interferometry. 2015 Fall Meeting of American Geophysical Union, S43D-2825

Gutenberg R, Richter CF (1944) Frequency of earthquakes in California. Bull Seismol Soc Am 34:185–188

Harris RA (1998) Introduction to special section: stress triggers, stress shadows, and implications for seismic hazard. J Geophys Res 103:347–358

Ingleby TF, Wright TJ, González PJ, Hooper AJ, John R Elliott JR (2015) Postseismic deformation following the April 2015 M7.8 Nepal earthquake measured using sentinel-1A interferometry. 2015 Fall Meeting of American Geophysical Union, S42C-08

Inouye W (1965) On the seismicity in the epicentral region and its neighborhood before the Niigata. Q J Seismol 29:139–144 **(in Japanese)**

Kisslinger C (1988) An experiment in earthquake prediction and the 7th May 1986 Andreanof Islands earthquake. Bull Seismol Soc Am 78:218–229

Kumazawa T, Ogata Y (2013) Quantitative description of induced seismic activity before and after the 2011 Tohoku-Oki earthquake by non-stationary ETAS models. J Geophys Res 118:6165–6182

Kumazawa T, Ogata Y, Toda S (2010) Precursory seismic anomalies and transient crustal deformation prior to the 2008 Mw = 6.9 Iwate-Miyagi Nairiku, Japan, earthquake. J Geophys Res 115:B103132. doi:10.1029/2010JB007567

Matsu'ura RS (1986) Precursory quiescence and recovery of aftershock activities before some large aftershocks. Bull Earthq Res Inst Univ Tokyo 61:1–65

Michael AJ, Blanpied ML, Brady SR, van der Elst N, Hardebeck J, Mayberry GC, Page MT, Smoczyk GM, Wein AM (2015). International aftershock forecasting: lessons from the Gorkha earthquake. 2015 Fall Meeting of American Geophysical Union, S42C-04

Ogata Y (1983) Estimation of the parameters in the modified Omori formula for aftershock frequencies by the maximum likelihood procedure. J Phys Earth 31:115–124

Ogata Y (1985) Statistical models for earthquake occurrences and residual analysis for point processes. Research Memo (Technical report) No 288, The Institute of Statistical Mathematics, Tokyo

Ogata Y (1988) Statistical models for earthquake occurrences and residual analysis for point processes. J Am Stat Assoc 83:9–27

Ogata Y (1989) Statistical model for standard seismicity and detection of anomalies by residual analysis. Tectonophysics 169:159–174

Ogata Y (1992) Detection of precursory relative quiescence before great earthquakes through a statistical model. J Geophys Res 97:19845–19871

Ogata Y (2001a) Increased probability of large earthquakes near aftershock regions with relative quiescence. J Geophys Res 106:8729–8744

Ogata Y (2001b) Exploratory analysis of earthquake clusters by likelihood-based trigger models. Festschrift Volume for Professor Vere-Jones. J Appl Probab 38A:202–212

Ogata Y (2004) Static triggering and statistical modelling. Rep Coord Comm Earthq Predict 72:631–637 **(in Japanese)**

Ogata Y (2005a) Detection of anomalous seismicity as a stress change sensor. J Geophys Res 110:B05S06. doi:10.1029/2004JB003245

Ogata Y (2005b) Synchronous seismicity changes in and around the northern Japan preceding the 2003 Tokachi-oki earthquake of M8.0. J Geophys Res 110:B08305. doi:10.1029/2004JB003323

Ogata Y (2005c) Relative quiescence reported before the occurrence of the largest aftershock (M5.8) in the aftershocks of the 2005 earthquake of M7.0 at the western Fukuoka, Kyushu, and possible scenarios of precursory slips considered for the stress-shadow covering the aftershock area. Rep Coord Comm Earthq Predict 74:529–535 **(in Japanese)**

Ogata Y (2006a) Monitoring of anomaly in the aftershock sequence of the 2005 earthquake of M7.0 off coast of the western Fukuoka, Japan, by the ETAS model. Geophys Res Lett 33:L01303. doi:10.1029/2005GL024405

Ogata Y (2006b) Seismicity anomaly scenario prior to the major recurrent earthquakes off the east coast of Miyagi Prefecture, northern Japan. Tectonophysics 424:291–306. doi:10.1016/j.tecto.2006.03.038

Ogata Y (2006c) Statistical analysis of seismicity—updated version (SASeis2006) Ver. 2. Computer science monographs no. 33. The Institute of Statistical Mathematics, Tokyo. http://www.ism.ac.jp/~ogata/Ssg/ssg_softwares.html

Ogata Y (2007) Seismicity and geodetic anomalies in a wide area preceding the Niigata-Ken-Chuetsu earthquake of 23 October 2004, central Japan. J Geophys Res 112:B10301. doi:10.1029/2006JB004697
Ogata Y (2010a) Space-time heterogeneity in aftershock activity. Geophys J Int 181(3):1575–1592. doi:10.1111/j.1365-246X.2010.04542.x
Ogata Y (2010b) Anomalies of seismic activity and transient crustal deformations preceding the 2005 M7.0 earthquake west of Fukuoka. Pure appl Geophys 167(8–9):1115–1127. doi:10.1007/s00024-010-0096-y
Ogata Y (2011) Pre-seismic anomalies in seismicity and crustal deformation: case studies of the 2007 Noto Hanto earthquake of M6.9 and the 2007 Chuetsu-oki earthquake of M6.8 after the 2004 Chuetsu earthquake of M6.8. Geophys J Int 186:331–348
Ogata Y (2013) A prospect of earthquake prediction research. Stat Sci 28(4):521–541. doi:10.1214/13-STS439
Ogata Y (2015) Monitoring seismicity anomalies by statistical models. Rep Coord Comm Earthq Predict 94:412–423. http://cais.gsi.go.jp/YOCHIREN/report/kaihou94/12_08.pdf
Ogata Y, Katsura K (1993) Analysis of temporal and spatial heterogeneity of magnitude frequency distribution inferred from earthquake catalogues. Geophys J Int 113:727–738
Ogata Y, Katsura K (2006) Immediate and updated forecasting of aftershock hazard. Geophys Res Lett 33(10):L10305
Ogata Y, Toda S (2010) Bridging great earthquake doublets through silent slip: on- and off-fault aftershocks of the 2006 Kuril Island subduction earthquake toggled by a slow slip on the outer rise normal fault the 2007 great earthquake. J Geophys Res 115:B06318. doi:10.1029/2009JB006777
Ogata Y, Jones LM, Toda S (2003) When and where the aftershock activity was depressed: contrasting decay patterns of the proximate large earthquakes in southern California. J Geophys Res 108(B6):2318. doi:10.1029/2002JB002009
Ohtake M, Matumoto T, Latham GV (1977) Seismicity gap near Oaxaca, southern Mexico as a probable precursor to a large earthquake. Pure appl Geophys 115:375–385
Omi T, Ogata Y, Hirata Y, Aihara K (2013) Forecasting large aftershocks within one day after the main shock. Sci Rep 3:2218
Omi T, Ogata Y, Hirata Y, Aihara K (2014a) Estimating the ETAS model from an early aftershock sequence. Geophys Res Lett 41:850–857
Omi T, Ogata Y, Hirata Y, Aihara K (2014b) Intermediate-term forecasting of aftershocks from an early aftershock sequence: Bayesian and ensemble forecasting approaches. J Geophys Res 120:2561–2578. doi:10.1002/2014JB011456
Omori F (1894) On the aftershocks of earthquake. J Coll Sci Imp Univ Tokyo 7:111–200
Page M, Hardebeck JL, Felzer K, Michael A (2015) Progress towards improved global aftershock forecasts. In: 2015 SCEC annual meeting proceedings, poster: 062
Parzen E, Tanabe K, Kitagawa G (eds) (1998) Selected papers of Hirotugu Akaike. Springer, Tokyo
Reasenberg PA, Jones LM (1989) Earthquake hazard after a main shock in California. Science 243(4895):1173–1176
Tsuruoka H (1996) Development of seismicity analysis software on workstation. Tech Res Rep, vol 2. Earthquake Res Inst, Univ Tokyo, Tokyo, pp 34–42 **(in Japanese)**
Tsuruoka H, Ogata Y (2015a) Development of seismicity analysis software: TSEIS–ETAS module implementation. In: 9th international workshop on statistical seismology (StatSei9), Arcona Hotel am Havelufer, Potsdam, Germany, 17 June 2015. https://statsei9.quake.gfz-potsdam.de/doku.php?id=13_presentations:start
Tsuruoka H, Ogata Y (2015b) Development of seismicity analysis tool XETAS. J Seismol Soc Jpn. Programme and abstract, the Seismological Society of Japan, 2015, Fall meeting, S09-P01, Kobe, Japan, 26 October 2015: Zisin (II) **(in preparation)**
Utsu T (1961) A statistical study on the occurrence of aftershocks. Geophys Mag 30:521–605
Utsu T (1968) Seismic activity in Hokkaido and its vicinity. Geophys Bull Hokkaido Univ 20:51–75. http://eprints.lib.hokudai.ac.jp/dspace/bitstream/2115/13944/1/20_p51-75.pdf **(in Japanese)**
Utsu T (1970) Aftershocks and earthquake statistics (II)—further investigation of aftershocks and other earthquake sequences based on a new classification of earthquake sequences. J Fac Sci Hokkaido Univ Ser 73:197–266. http://eprints.lib.hokudai.ac.jp/dspace/handle/2115/8684
Utsu T (1979) Calculation of the probability of success of an earthquake prediction (In the case of Izu-Oshima-Kinkai earthquake of 1978). Rep Coord Comm Earthq Predict 21:164–166. http://cais.gsi.go.jp/YOCHIREN/report/kaihou21/07_04.pdf
Utsu T, Ogata Y and Matsu'ura RS (1995) The centenary of the Omori formula for a decay law of aftershock activity. J Phys Earth 43:1–33. https://www.jstage.jst.go.jp/article/jpe1952/43/1/43_1_1/_pdf
Wyss M, Burford RO (1987) A predicted earthquake on the San Andreas fault, California. Nature 329:323–325
Zhang G, Hetland E, Shan X (2015) Slip in the 2015 Mw 7.9 Gorkha and Mw 7.3 Kodari, Nepal, earthquakes revealed by seismic and geodetic data. Seismol Res Lett 86(6). doi:10.1785/0220150139